Available online at www.sciencedirect.com
ScienceDirect
Advances in Space Research 42 (2008) 424–430
ADVANCES IN SPACE RESEARCH (a COSPAR publication)
www.elsevier.com/locate/asr

Enhancing the ATIC charge resolution

T.G. Guzik [g,*], J.H. Adams Jr. [a], H.S. Ahn [b], G.L. Bashindzhagyan [c], K.E. Batkov [c], J. Chang [d,e], M. Christl [a], A.R. Fazely [f], O. Ganel [b], R.M. Gunashingha [f], J. Isbert [g], K.C. Kim [b], E.N. Kouznetsov [c], M.I. Panasyuk [c], A.D. Panov [c], W.K.H. Schmidt [e], E.S. Seo [b], N.V. Sokolskaya [c], J.W. Watts [a], J.P. Wefel [g], J. Wu [b], V.I. Zatsepin [c]

[a] *NASA Marshall Space Flight Center, Huntsville, AL 35812, USA*
[b] *University of Maryland, Institute for Physical Science & Technology, College Park, MD 20742, USA*
[c] *Skobeltsyn Institute of Nuclear Physics, Moscow State University, Moscow 119899, Russia*
[d] *Purple Mountain Observatory, Chinese Academy of Sciences, Nanjing 210008, China*
[e] *Max-Planck Institute for Solar System Research, Katlenburg-Lindau 37191, Germany*
[f] *Southern University, Department of Physics, Baton Rouge, LA 70813, USA*
[g] *Louisiana State University, Department of Physics and Astronomy, Baton Rouge, LA 70803, USA*

Received 1 December 2006; received in revised form 13 April 2007; accepted 9 August 2007

Abstract

The Advanced Thin Ionization Calorimeter (ATIC) experiment is designed to investigate the charge composition and energy spectra of primary cosmic rays over the energy range from about 10^{11} to 10^{14} eV during Long Duration Balloon (LDB) flights from McMurdo, Antarctica. Currently, analysis from the ATIC-1 test flight and ATIC-2 science flight is underway and preparation for a second science flight is in progress. Charge identification of the incident cosmic ray is accomplished, primarily, by a pixilated Silicon Matrix detector located at the very top of the instrument. While it has been shown that the Silicon Matrix detector provides good charge identification even in the presence of electromagnetic shower backscatter from the calorimeter, the detector only measures the charge once. In this paper, we examine use of the top scintillator hodoscope detector to provide a second measure of the cosmic ray charge and, thus, improve the ATIC charge identification.

Keywords: Ballooning; ATIC; Particle detectors; Hodoscope; Charge resolution

1. Introduction

Most of our knowledge of cosmic rays derives from studying the particles at low energy, i.e., below 10's of GeV/nucleon. Above this energy, the cosmic rays follow a power-law energy spectrum, indicative of what is derived from first order Fermi acceleration operating at a shock wave discontinuity (Ellison et al., 1994). The current results show a featureless energy spectrum up to a few $\times 10^{15}$ eV where the spectral slope steepens. This feature, discovered over 40 years ago from ground based air shower experiments, is called the "knee" (Kulikov and Khristiansen, 1959). Its importance in understanding the origin and history of the cosmic rays has been stressed for many years, since the "knee" points to the astrophysics to unravel this part of the cosmic ray mystery. Theory supports this conclusion since it is in the high energy region that "signature" effects of the acceleration process may be observed.

The Advanced Thin Ionization Calorimeter (ATIC) Balloon Experiment was designed to investigate the composition and energy spectra of cosmic rays in this high energy ($>10^{11}$ eV) regime. The instrument consists of a pixilated Silicon Matrix (SiM) detector for determining the cosmic ray charge, three plastic scintillator hodoscopes (S1, S2, and S3) for defining the instrument geometry and initial

* Corresponding author. Tel.: +1 225 578 8597; fax: +1 225 578 1222.
E-mail address: guzik@phunds.phys.lsu.edu (T.G. Guzik).

0273-1177/$34.00 © 2007 COSPAR. Published by Elsevier Ltd. All rights reserved.
doi:10.1016/j.asr.2007.08.017

event trigger, a carbon target to induce hadron interactions, plus a fully active Bismuth Germanate (BGO) calorimeter to measure the particle energy (Guzik et al., 1999). ATIC addresses the high energy frontier, i.e., direct measurements to as high an energy as possible from balloon platforms (Panov et al., 2006). Due to the power-law energy spectrum, the high energy limit is set by exposure. Consequently, ATIC was designed specifically for a series of Long Duration Balloon flights from McMurdo, Antarctica (Guzik et al., 2003).

ATIC has had three launches from McMurdo. The ATIC-1 test flight in 2000 achieved about 15 days at float and was used to validate instrument performance (Wefel, 2001; Seo, 2001). The lessons learned during the test flight were used to improve the instrument in preparation for its first science flight (ATIC-2) in 2002. ATIC-2 was launched on 29 December 2002 and remained at float for 19 days during which we obtained ~17 days of good, analyzable data. ATIC-3, in 2005, was intended to be a second science flight and preparations for launch went well. Fig. 1 shows ATIC-3 on the launch pad waiting for release of the balloon. Shortly after launch, unfortunately, a problem with the balloon became apparent and the flight had to be terminated. The payload was successfully recovered and is now being prepared for a re-flight in 2007.

One of the primary technical objectives for ATIC is to identify the incident cosmic ray charge in the presence of minimum ionizing particles generated during shower development in the calorimeter and backscattered to the charge detector. The highly pixilated SiM was designed to achieve this objective and, in general, has been shown to have good charge resolution (Adams et al., 2001a; Zatsepin et al., 2004). However, the SiM provides only one measure of the cosmic ray charge. Here we examine the charge resolution in the top hodoscope detector (S1) and determine the extent that measurements in both the SiM and S1 can be used to improve the ATIC cosmic ray element identification.

Fig. 1. The ATIC payload being readied for launch on December 19, 2005.

2. The ATIC instrument

The only practical method of energy determination over a broad energy range for $Z \geqslant 1$ is ionization calorimetry (Fabjan, 1987; Isbert et al., 1995; Wigmans, 2000). In an ionization calorimeter, a particle's energy is deposited inside a medium via a cascade of nuclear and electromagnetic interactions. At each step of the cascade, the energy of the primary particle is sub-divided among many secondary particles. The area under the curve of ionization energy versus depth in the medium provides a measure of the particle energy. The energy resolution of a finite calorimeter depends on the fluctuations in the energy transferred to the pions, particularly in the first interaction. Practical calorimeters for balloon applications must necessarily be limited in thickness, in order to have a reasonable cross sectional area, i.e., geometrical factor, and a "flyable" weight. In a thin calorimeter to measure cosmic rays, the primary nucleus must undergo at least one inelastic interaction, and deposited energy must be measured with good resolution.

ATIC uses a calorimeter based upon fully active Bismuth Germanate (BGO) scintillating crystals (1.12 cm per r.l.) following a 30 cm carbon target (25 cm per r.l.) (Isbert et al., 2002; Ganel et al., 2005). The incident particle interacts in the carbon, but the majority of the shower develops in the BGO. A schematic of the ATIC instrument, with a simulated event superposed (Wang et al., 1997) is shown in Fig. 2. The calorimeter itself is segmented with each layer consisting of 40 crystals each of which has dimensions $2.5 \times 2.5 \times 25$ cm and is viewed by a Hamamatsu R5611 photomultiplier tube. Alternate layers are assembled orthogonally giving x–y pairs that together determine the axis of the shower. For ATIC-1 and ATIC-2 eight such layers were used to conserve weight, giving a calorimeter depth of 17.9 X_o. For the next ATIC flight ten BGO layers or $X_o \approx 22$ will be used for the calorimeter.

The instrument must also determine the charge of the incident particle and measure its trajectory through the apparatus. At the top of the instrument is a silicon detector to determine the charge of the incident particle (Adams

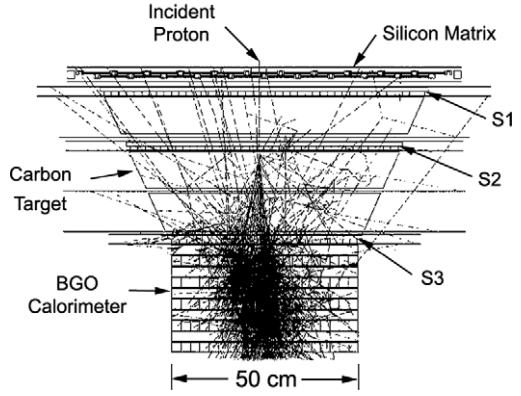

Fig. 2. A schematic of the ATIC instrument with a simulated event.

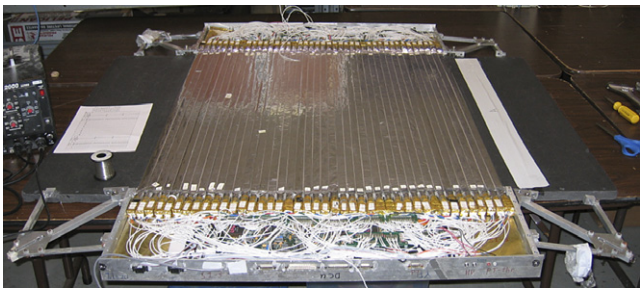

Fig. 3. One layer of plastic scintillator strips making up the S1 hodoscope.

et al., 1999a, 2001a; Adams, 2001b). In a calorimeter, there is always some "backsplash" of particles emitted into the backward hemisphere that may confuse the charge measurement (cf. Fig. 2). To resolve this problem, the Silicon Matrix includes 4480 "pixels" of 2×1.5 cm area mounted on offset ladders, which allows separation of the backscatter noise from the incident particle signal. The total active area of the Silicon Matrix is 0.95×1.05 m.

In addition, crossed plastic scintillator strip hodoscope layers are located at the top, bottom, and within the carbon target (S1, S2, and S3 in Fig. 2) to provide triggering (geometry definition) and auxiliary charge information as well as tracking information to be combined with the location of the shower core from the calorimeter (Ganel and Seo, 2000). Each hodoscope is composed of two orthogonal layers of similar construction though the length and number of strips varies with the position of the layer in the instrument. One such hodoscope layer is shown in Fig. 3. For S1, 84 strips of Bicron BC-408 of dimensions $2 \times 1 \times 88.2$ cm are used, while S2 includes 70 strips 74.2 cm long and S3 has 48 strips that are 52.4 cm long. Each strip has a Hamamatsu R5611 on each end of each strip. Finally, 16 channel, 16 bit CR-1 application-specific integrated circuits (ASIC) (Adams et al., 1999b) are used for the Silicon Matrix readout while ASICs based on the design used for the ACE mission (Cook et al., 1993), including 16 input channels, two "trigger" output signals as well as 12 bit digitized pulse heights are used for the BGO and hodoscope readout.

3. The ATIC charge resolution

To date only the Silicon Matrix detector has been used in the ATIC flight data analysis to determine the incident particle charge. While this detector has performed well, additional information from the S1 hodoscope could be used to enhance the overall charge resolution. However, to use S1 for this purpose, calibrations to convert the raw pulse heights into charge units had to be performed on individual strips.

3.1. The Silicon Matrix performance

The SiM detector is composed of 4480 individual silicon pixels to reduce the probability that the single pixel "hit" by the incident cosmic ray will also have multiple backscatter particle signals. To reduce on-board data volume only those pixels with signals above a preset threshold are readout. This threshold is set relative to the pixel pedestal value which can vary as a function of temperature. Thus, during the ATIC flights the pedestal of each SiM pixel is automatically measured every 6 min and used to adjust the readout threshold. In addition, each silicon pixel and associated electronics readout channel are slightly different, which must be calibrated. These calibrations and temperature adjustments were accomplished and applied to the flight data, resulting in outputs normalized to the same scale.

Once the particle trajectory is determined and the "hit" pixel for each event identified, values for all events can be summed into a histogram. The resulting charge histogram, Fig. 4, shows the $Z = 1$–5 region (top) and the bottom panel is for $Z = 4$–26. Fig. 4 shows a clear separation between H and He, plus charge peaks at C, O, Ne, Mg, Si, and Fe. The distribution widths in the CNO region are in the range 0.35–0.45 charge units. The charge peaks remain separated up to incident particle energies of 100 TeV.

Each pixel is 380 μm thick and fluctuations in the energy deposit produce a Vavalov tail to the distributions. Further broadening results from the delta rays produced in the surrounding structure as described in detail by Zatsepin et al. (2004). As these energy deposit fluctuations are random, multiple measurements of the incident particle charge would improve element identification. Alternate SiM "ladders" (strips of silicon pixels) are actually staggered vertically by a few centimeters, leaving open the possibility

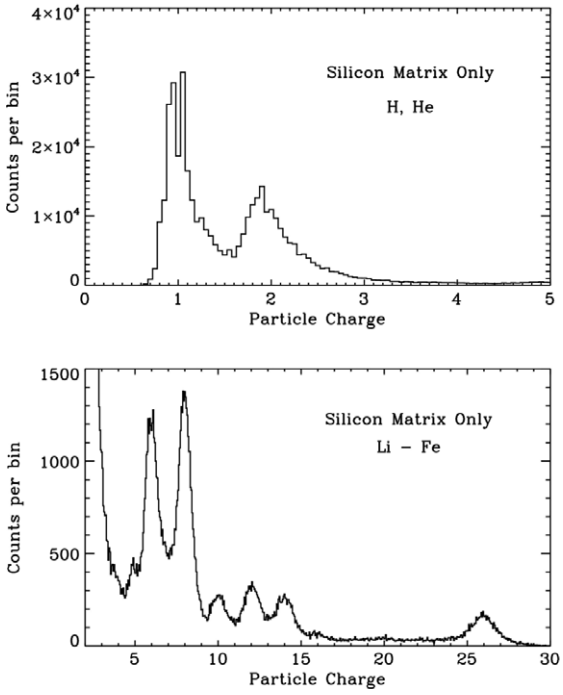

Fig. 4. Flight data charge histogram using only the Silicon Matrix for H–He (top) and Li–Fe (bottom).

that some cosmic rays will pass through two pixels. However, these "two hit" trajectories are only a small fraction (~10%) of the total ATIC geometry making it impractical to rely upon multiple measurements in the SiM detector. However, the "two hit" events do demonstrate that a reduction in the peak widths is possible (Zatsepin et al., 2004). What is discussed here is the use of another detector, S1, which covers the same geometry as the SiM to obtain a second charge measurement for the cosmic rays.

3.2. Calibration of the S1 hodoscope

Obtaining a particle charge value from the raw S1 pulse height is a multiple step operation involving, (1) correcting the rate dependent ADC baseline shift, (2) establishing the energy scale using ground level muons, (3) determining the relative ratio between the different photomultiplier (PMT) readout gains, (4) identifying the particle trajectory and correcting for pathlength differences, (5) accounting for scintillator attenuation length effects, and (6) determining the charge to energy deposit relationship for each individual hodoscope strip. Following these steps the charge determined in S1 and the SiM can be averaged and analyzed to determine the level of improvement in element identification.

Analysis of the ATIC-1 and ATIC-2 raw datasets display frequent baseline shifts in the hodoscope and calorimeter pulse height that have the effect of confusing the energy deposit measurement. As the level of the baseline shift is correlated across all channels of the same ASIC, we were able to use extra channels that were disconnected from detector signals to "trace" the baseline shift on an event by event basis. These measured shifts were then applied to every hodoscope and calorimeter channel of every event to fully correct the problem.

The ATIC detectors and electronics were designed to be sensitive to minimum ionizing ground level muons. These muons result from interactions of cosmic rays in Earth's upper atmosphere, have well known angular and energy distributions, are highly penetrating and provide a convenient "standard" source of high energy particles anywhere on the planet. Thus, ATIC incorporates a particular trigger mode to allow the instrument to collect muon data in order to validate detector performance and diagnose problems in the laboratory or on the flight line. As muons are minimum ionizing, the same dataset can be used to establish the initial energy scale for the instrument. Prior to launch ATIC collects muon data for 24–36 h. This provides a reasonable population of particles passing through each detector segment. Following flight, histograms of the muon energy deposit for each detector channel are produced and fit to determine the pulse height corresponding to the average energy deposit. This average is about 2.1 MeV for a hodoscope strip and about 23 MeV for a BGO crystal. Such a histogram for a single hodoscope strip is shown in panel (a) of Fig. 5. Here the fit has determined that the histogram peak is at a pulse height of 110 and, consequently, the

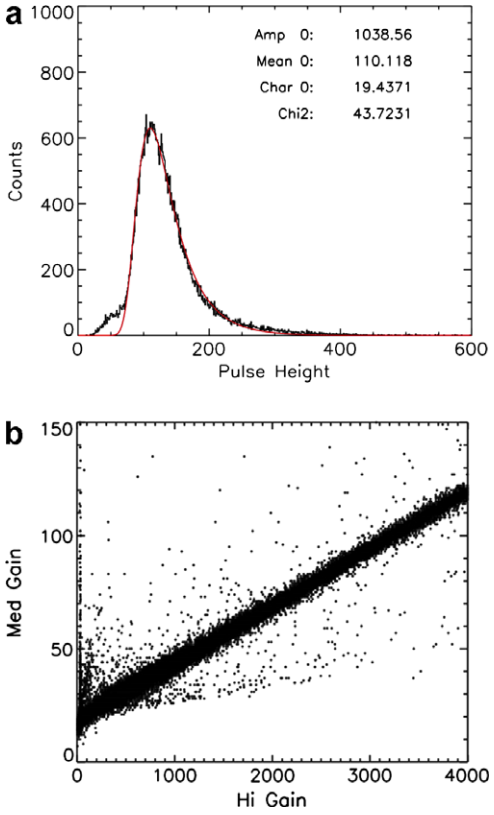

Fig. 5. Typical muon distribution and fit (a) and relationship between two gain ranges (b).

energy scale of this gain range would be about 19 keV per ADC channel.

For ATIC to provide measurements of H to Fe over an energy range of ~100 GeV to 100 TeV every hodoscope and calorimeter detector segment also needs to cover a broad dynamic range. This is accomplished by picking off different PMT dynodes and connecting each of these to a different electronic readout channel. For the hodoscope two such pickoffs (high and low) are used for each PMT, while for the calorimeter three (high, medium and low) are used. The high gain (high amplification) range provides the maximum resolution for small energy deposits, such as that generated by minimum ionizing muons or protons, while the lower gain ranges produce a measurable signal for the high energy deposits that would saturate the high gain range. Thus, the data for the muon energy deposit histogram in Fig. 5(a) are from the high gain range, and the energy scale so determined will not apply to the lower gain ranges. Rather, the ratio between gain ranges must be determined from flight data and used to extend the energy scale to the low ranges. Panel (b) of Fig. 5 shows a plot of the signal from the medium (y axis) and high (x axis) gain range of a single calorimeter PMT. Note that the high gain values in the plot cover the full 12 bit range of the ADC while only the lower ~3% of the medium gain range is used. Similar plots were done for every pair of gain ranges for every hodoscope and calorimeter PMT and used to establish the energy scale for each gain range. The detector

segment energy deposit assignment is then determined by picking the highest gain range (i.e., highest "resolution") that is not saturated.

Incident cosmic rays impact ATIC isotropically and can enter ATIC with a maximum angle somewhat greater than 50°, although the average angle for all particles is closer to about 24°. It is therefore necessary to determine the particle trajectory through ATIC to correct the pathlength to normal incidence and to identify the SiM pixel and S1 strip that is "hit" by the incident particle. As mentioned in Section 2, alternate hodoscope and calorimeter layers are rotated by 90° to give a (X,Z) or (Y,Z) coordinate for the trajectory where Z is along the vertical axis of the instrument. For ATIC-2 there are a maximum of 7 such coordinates (four from the calorimeter and three from the hodoscopes) in each plane. For this analysis we further require a minimum energy deposit in a calorimeter layer to assure that a shower core has developed. The "hit" coordinate in each layer is determined by weighting the detector segment position by the energy deposit. The trajectory is then determined from fits in both the (X,Z) and (Y,Z) planes, which is then used to identify the "hit" detector segments and to correct the energy deposit for pathlength differences. These data can then be correlated to obtain the S1 charge calibration.

The light generated in the plastic scintillator by the passage of the high energy particle will be attenuated as it propagates to the PMTs on each end of the strip. For the BC-408 material making up the hodoscope strips this bulk attenuation length is 380 cm. Since the S1 strips are almost 90 cm long we, therefore, expect to see the PMT signal to show some dependence on the particle "hit" position along the strip. To minimize this "attenuation effect" the geometric mean of the signal from both tubes at the each end of the strip was used in the final analysis.

A further complication resulted from an on-board failure during the ATIC-2 flight. The nominal voltage applied to the PMTs on both S1 hodoscope layers is about 980 VDC and pre-launch calibrations, such as the muon data used for setting the energy scale, are done at this voltage. At this voltage the high gain range would be sensitive to H, He, and saturate at about C, while the low gain range would "see" B through Fe. However, shortly after the ATIC-2 launch an on-board failure required that we reduce the S1X layer voltage to about 600 VDC. This had the effect of reducing the gain in this layer by about a factor of 16, resulting in moving signals from He to Fe into the high gain range and bringing most of the H to below threshold. The S1Y layer was not affected by this failure and remained at its nominal operating voltage throughout the flight.

The final stage of the S1 charge calibration was accomplished by plotting for each hodoscope strip the charge determined from the SiM versus the energy deposited in the strip. This correlation, as shown in Fig. 6 for two S1 strips, was found to vary from strip to strip, and is likely due to differences in the detector material and readout electronics not easily accounted for with the standard calibrations. The correlation plots, however, show clear grouping at B, C, N, O, Ne, Mg, Si, and Fe and, on a magnified scale, H (for S1Y) and He. This information was used to determine a charge calibration curve for each of the 42 strips per S1 layer producing a normalized charge scale across the detector. The end result was that either S1Y or S1X can be used to determine incident particle charge (with the exception of H in S1X) and both cover the geometry of the SiM.

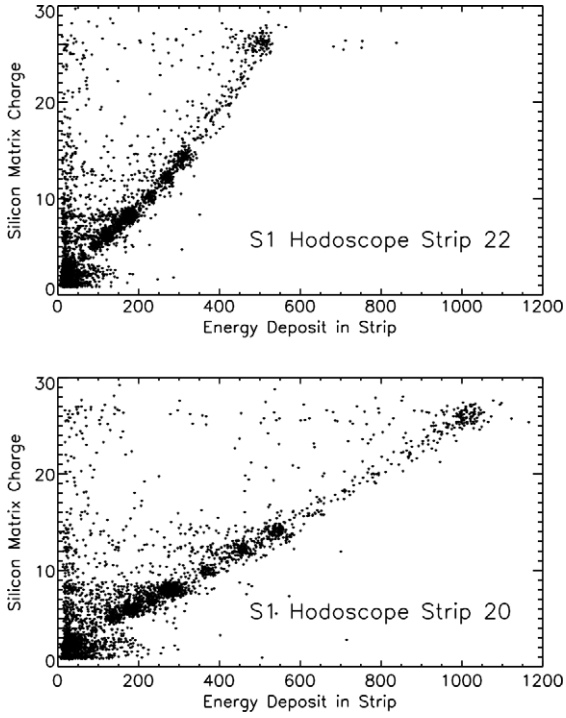

Fig. 6. Two strips in S1 illustrating the strip-to-strip variation in charge response.

3.3. The combined detector charge resolution

With both layers of S1 calibrated, an average value for the particle charge can be determined and compared with that determined from the SiM. Such a correlation plot is shown in Fig. 7 with the SiM charge on the y-axis and the S1 charge on the x-axis. Excellent charge resolution is evident in this plot. Not only are C, N, O, Ne, Mg, Si, and Fe groups clearly seen, but the He tail is repressed allowing Li, Be, and B to emerge and faint peaks at S, Ar, and Ca are visible. As H is mostly below threshold in S1X, He but not H is apparent in the plot. Cutting on lines parallel to the diagonal to eliminate particles that interact within the instrument, then averaging the SiM, S1Y, and S1X charges together and histograming the result produces the lower panel of Fig. 8 for Li to Fe. A similar process using only the SiM and S1Y charges produces the upper panel of Fig. 8 for H and He. When compared with the SiM only charge resolution (Fig. 4), Fig. 8 shows dramatic

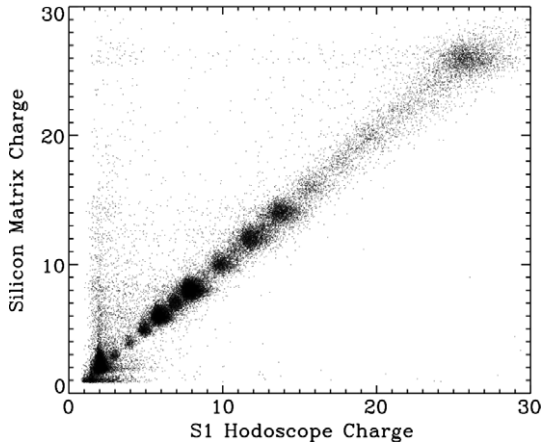

Fig. 7. Scatter plot showing the correlation between charge determined in the Silicon Matrix versus that determined with S1.

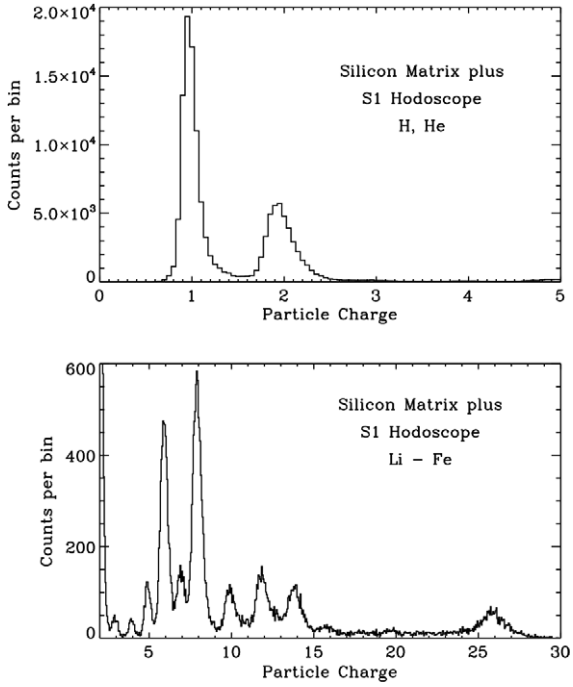

Fig. 8. Charge histogram using both the Silicon Matrix and S1.

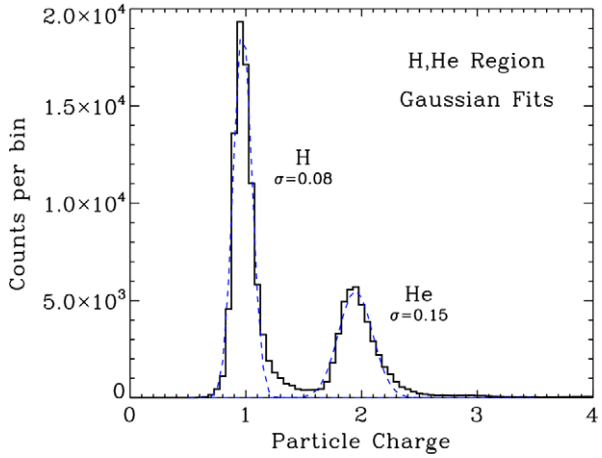

Fig. 9. Gaussian distribution fits for the H and He charge histograms.

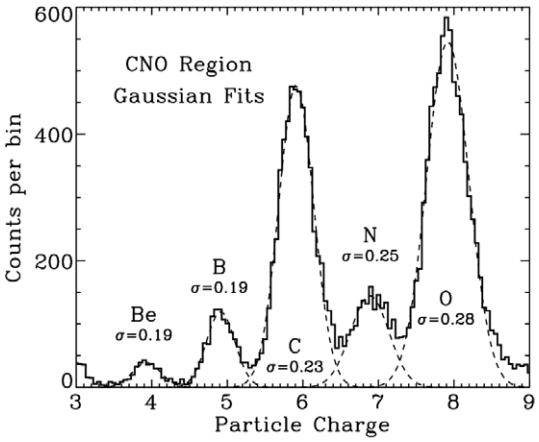

Fig. 10. Gaussian distribution fits for the Be to O charge histograms.

improvement. For H and He the high end tails in the distributions are repressed, and the peaks have narrowed, resulting in significantly reduced misidentification of H as He. For the heavier ions Be is clearly resolved, B is separated from C and a peak for N is apparent. In addition, the Ne, Mg, and Si peaks have narrowed, though peaks for the odd Z nuclei in this region have not emerged.

To quantify the charge resolution improvement we can fit selected charge peaks with gaussian distributions and determine the σ values. This was done for H and He and is shown in Fig. 9 where the fit distributions are the dashed curves. The resulting gaussian widths are $\sigma = 0.08$ charge units for H and $\sigma = 0.15$ for helium. Even though these widths indicate that H and He are well separated there is still a residual tail on the distributions for both elements. Fig. 10 shows similar fits for Be, B, C, N, and O. In this case the gaussian fits reproduce the histogram peaks with little evidence of tails. Further, the measured distribution widths vary from 0.19 to 0.28; a 40% to 50% improvement relative to using only the SiM for particle charge identification.

4. Conclusions

Here we have been able to show that the S1 hodoscope can provide an independent measure of the incident particle charge. In fact, each of the two layers making up S1 can provide a charge measurement and cover most of the ATIC geometrical factor. The exception to this later statement is that due to a high voltage limitation on-board ATIC-2, one of the S1 layers has reduced sensitivity to protons. Combining the particle charge determined in the Silicon Matrix with that determined in S1 results in almost a factor of two improvement in charge resolution for elements up to at least Oxygen. In addition, contamination of helium due to misidentified protons is reduced and the full geometry of ATIC can be

used. This enhanced charge resolution opens up new possibilities for the ATIC data analysis including improved H, He spectra determination, enhanced separation of background γ rays from cosmic ray electrons and high energy B/C ratio results. Finally, extending this analysis to the S2 and S3 hodoscopes may improve our ability to localize the hadron interaction point in the carbon target material and possibly further enhance the ATIC charge resolution.

Acknowledgements

The ATIC project is supported in the USA by NASA Supporting Research and Technology (NNG04WC10G, NNG04WC12G, NNG04WC06G), in Russia by the Russian Foundation for Basic Research (02-02-16545, 05-02-16222), and in China by the Ministry of Science and Technology of China (2002CB713905, 2002AA732021, 2002AA732022).

References

Adams Jr., J.H., Ampe, J., Bashindzhagyan, G. Silicon matrix detector for ATIC, in: Proceedings of the 26th Int. Cosmic Ray Conf., Salt Lake City, 5, pp. 76–79, 1999a.

Adams Jr., J.H., Ampe, J., Bashindzhagyan, G. The CR-1 chip: custom VLSI circuitry for cosmic rays, in: Proceedings of the 26th Int. Cosmic Ray Conf. Salt Lake City, 5, pp. 69–72, 1999b.

Adams Jr., J.H., Bashindzhagyan, G.L., Zatsepin, V.I., et al. The silicon matrix as a charge detector for the ATIC experiment. Instrum. Exp. Tech. 44, 455–461, 2001a.

Adams Jr., J.H., for the ATIC collaboration. Preliminary results from the first flight of ATIC: the silicon matrix, in: Proceedings of the 27th Intl. Cosmic Ray Conf., Hamburg, 6, pp. 2127–2130, 2001b.

Cook, W.R., Cummings, A.C., Kecman, B., Mewaldt, R.A., Aalami, D., Kleinfelder, S.A., Marshall, J.H. Custom analog VLSI for the advanced composition explorer (ACE), Small Instruments for Space Physics/Proceedings of the Small Instrument Workshop, Pasadena, CA, 7–19, 1993.

Ellison, D.C., Reynolds, S.P., Borkowshi, K., et al. Supernova remnants and the physics of strong shock waves. Publ. Astron. Soc. Pacific 106, 780–797, 1994.

Fabjan, C. Calorimetry in high-energy physics, in: Ferbel, T. (Ed.), Experimental Techniques in High Energy Physics. Addison-Wesley Publishing Company, Inc., Menlo Park, CA, pp. 257–324, 1987.

Ganel, O., Seo, E.S. Improving cosmic ray composition determination through better tracking. Adv. Space Res. 26, 1835–1838, 2000.

Ganel, O., Adams, J.H., Ahn, H.S., et al. Beam test of the balloon-borne ATIC experiment. Nucl. Instrum. Methods A 552, 409–419, 2005.

Guzik, T.G., Adams Jr., J.H., Ampe, J. The advanced thin ionization calorimeter (ATIC) for studies of high energy cosmic rays, in: Proceedings of the 26th Int. Cosmic Ray Conf., Salt Lake City, 5, pp. 9–12, 1999.

Guzik, T.G., Adams Jr., J.H., Ahn, H.S., et al. The ATIC long duration balloon project. Adv. Space Res. 33, 1763–1770, 2003.

Isbert, J., Guzik, T.G., Lockwood, R., McDonald, B. Seo, E.S. Wefel, J.P. Advanced thin ionization calorimeter (ATIC), in: Proceedings of the 24th Int. Cosmic Ray Conf., Rome, 3, pp. 719–722. 1995.

Isbert, J. Case, G. Granger, D. ATIC a balloon borne calorimeter for cosmic ray measurements, in: Zhu, R.-Y. (Ed.), Proceedings of the 10th Intl. Conference on Calorimetry in Particle Physics, World Scientific, Singapore, pp. 89–94, 2002.

Kulikov, G.V., Khristiansen, G.B. Sov. Phys. JETP 35, 441, 1959.

Panov, A.D., Adams, J.H., Ahn, H.S., et al. The energy spectra of heavy nuclei measured by the ATIC experiment. Adv. Space Res. 37, 1944–1949, 2006.

Seo, E.S., for the ATIC collaboration. Preliminary results from the first flight of ATIC, in: Proceedings of the 27th Intl. Cosmic Ray Conf., Hamburg, 5, pp. 1601–1604, 2001.

Wang, J.Z., Seo, Adams Jr., J.H. Cosmic ray shower simulation and reconstruction for the ATIC experiment, in: Proceedings of the 25th Intl. Cosmic Ray Conf., Durban, 5, pp. 5–8, 1997.

Wefel, J.P., for the ATIC collaboration. The ATIC experiment: first balloon flight, in: Proceedings of the 27th Intl. Cosmic Ray Conf., Hamburg, 6, pp. 2111–2114, 2001.

Wigmans, R. Calorimetry: Energy Measurement in Particle Physics, International Series on Monographs on Physics, 107. Oxford University Press, Oxford, England, ISBN 978-0-19-850296-8, 2000.

Zatsepin, V.I., Adams, J.H., Ahn, H.S., et al. The silicon matrix as a charge detector in the ATIC eperiment. Nucl. Instrum. Methods A 524, 195–207, 2004.